RESEARCH ARTICLE | NOVEMBER 15 1991

Reaction paths and free energy profiles for conformational transitions: An internal coordinate approach

Themis Lazaridis; Douglas J. Tobias; Charles L. Brooks, III; Michael E. Paulaitis

J. Chem. Phys. 95, 7612–7625 (1991)
https://doi.org/10.1063/1.461335

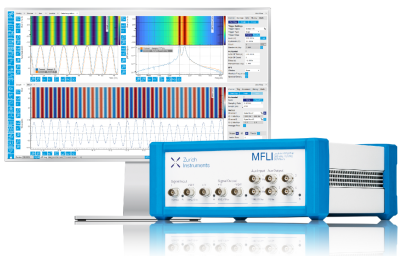

Reaction paths and free energy profiles for conformational transitions: An internal coordinate approach

Themis Lazaridis
Department of Chemical Engineering, University of Delaware, Newark, Delaware 19716

Douglas J. Tobias[a] and Charles L. Brooks III
Department of Chemistry, Carnegie Mellon University, Pittsburgh, Pennsylvania 15213

Michael E. Paulaitis[b]
Department of Chemical Engineering, University of Delaware, Newark, Delaware 19716

(Received 20 May 1991; accepted 2 August 1991)

A new approach is proposed for the determination of transition states and reaction paths for conformational transitions. The method makes use of adiabatic energy surfaces in the space of "essential" degrees of freedom of the molecule. The reduced dimensionality of this space, compared to the full Cartesian space, offers improved computational efficiency and should allow determination of exact reaction paths in systems much larger than those currently amenable to study in Cartesian space. A procedure to obtain reaction paths and free energy profiles in solution is also proposed. The free energy profile along the path in solution is calculated utilizing a free energy perturbation method with constrains and perturbations in internal coordinate space. Applications to a conformational transition of the alanine dipeptide and the folding transition of a model reverse turn in water are presented. For the reverse turn, the sequential flip of dihedral angles reported by Czerminsky and Elber on a similar peptide [J. Chem. Phys. **92**, 5580 (1990)] is also observed in the present calculations. The free energy of the extended form of the reverse turn in water is found to be lower than that for the folded conformation by about 3 Kcal/mol, in qualitative accord with previous umbrella sampling calculations.

I. INTRODUCTION

A distinguishing characteristic of macromolecules is their ability to adopt a large number of different conformations and to fluctuate between these conformations on a wide range of time scales.[1-3] In the case of biological macromolecules, and most notably proteins, conformational transitions are involved both in the folding process[3] and in structural fluctuations that accompany and are considered to be crucial for biological function.[4,5] In the realm of synthetic polymers, conformational transitions greatly influence the mechanical properties of these materials, such as the stress–strain behavior,[6] as well as the dynamic behavior of chains in solution.[7] Furthermore, the mechanism of mass transport through polymeric materials appears to be intimately related to the conformational mobility of the polymer chains.[8,9] Thus there is critical need to understand the mechanism of conformational transitions and develop methodologies for predicting their rates by theoretical and/or computational means.

Nonreactive processes, such as conformational transitions, that proceed without formation or breaking of covalent bonds, can be studied with molecular models based on empirical force fields (e.g., see Ref. 10), which, for activated processes, readily provide the energetic contributions to the free energy barriers. Furthermore, empirical energy functions, implemented in molecular dynamics simulations, implicitly reproduce entropic effects, provided that the simulations cover a multiple of the time scale of the process under study. Most conformational transitions of interest, however, occur on time scales much longer than simulation time scales and therefore cannot realistically be studied by conventional molecular dynamics simulations. In these cases the formalism of transition state theory,[11,12] in conjunction with free energy calculation techniques[13] promises to be the most viable alternative. In this approach, a reaction coordinate is first identified and the free energy profile along this reaction coordinate is calculated. The rate can then be extracted on the basis of transition state theory, with dynamic corrections obtained through "activated" molecular dynamics simulations.[11,14]

An implicit assumption in the above procedure is that the reaction coordinate for the conformational transition is known. In simple cases, the reaction coordinate can be approximated by a single internal coordinate or a simple geometrical parameter, such as the central dihedral angle in the *trans–gauche* isomerization of butane,[15-17] the difference between two dihedral angles for the rotation of a protein side chain,[14] or the distance from a surface opening for the escape of a ligand from the protein myoglobin.[18] In other cases, however, the transition is more complex and a more precise definition of the reaction coordinate must be implemented. The most widely accepted definition is the intrinsic reaction coordinate (IRC),[19,20] which is essentially a steepest descent path on the multidimensional potential energy surface of the molecule. So far, IRCs have been determined mostly on the quantum-mechanical energy surfaces of small, reactive systems [e.g., see Refs. 21 and 22]. The bottleneck in the

[a] Current address: Department of Chemistry, University of Pennsylvania, Philadelphia, Pennsylvania 19104.
[b] Author to whom correspondence should be addressed.

 0021-9606/91/227612-14$03.00

determination of the IRC is the location of the transition state, corresponding to a saddle point on the potential energy surface. Several algorithms have been proposed to this end [for a review, see Ref. 23]. Most of the methods employed recently are based on the algorithm of Cerjan and Miller,[24] which can efficiently locate saddle points without the need of a good initial guess.

The first application of techniques to determine transition states for the conformational processes of interest here was by Nguyen and Case, who determined transition states and energy minima for cyclo-octane and two dipeptides.[25] More recently, Elber and co-workers have devised methodologies for handling problems of larger scale, such as helix-to-coil transitions in peptides,[26–28] ligand diffusion in proteins,[29] or even global transitions in small proteins.[30] Elber has also developed a methodology to calculate the potential of mean force along an arbitrary reaction coordinate.[31]

In all previous work on multidimensional reaction coordinates for conformational processes, the molecular conformation has been described by the Cartesian coordinates of all the atoms in the system. This approach has the advantages of generality and simplicity, due to the Euclidean character of the Cartesian coordinate space. However, its major drawback is the large dimensionality of the problem ($3N$, where N is the number of atoms). The large dimensionality is particularly costly in the determination of the transition state, which requires diagonalization of the Hessian of the energy. This difficulty led Elber and co-workers to develop alternative methods, utilizing only first derivatives of the energy.[27,28]

Since conformational transitions involve primarily changes in dihedral angles, while the "stiff" degrees of freedom (bond lengths and angles) change only slightly during the process, the inclusion of all degrees of freedom in the calculation of reaction paths is highly inefficient. [Throughout this paper the terms "reaction path" (RP) and "reaction coordinate" (RC) will be used interchangeably.] One would expect that considerable computational effort could be saved by the use of internal coordinates. Moreover, internal coordinates provide a better physical description of molecular conformations.

In this work, we propose searching for transition states and the associated reaction coordinates in the space of "essential" angles involved in the conformational transition of interest. The major benefit from this approach is a large reduction in the dimensionality of conformational space. For example, there are two essential torsional angles for the alanine dipeptide, compared to 36 Cartesian coordinates (in a "polar hydrogen" representation). This reduction in dimensionality allows the use of rigorous search techniques for the transition states and ultimately the study of much larger systems.

Changes in the stiff degrees of freedom, although small, are energetically important, and therefore cannot be omitted. These changes can be efficiently taken into account by an "adiabatic approximation" which, during the transition, allows bond lengths and angles to fully relax to their optimal values for each set of essential torsional angles. Thus the proposed method can be thought of as an extension of the familiar "adiabatic mapping" technique[32] to an arbitrary number of dimensions: The essential torsional angles ("mapping coordinates") are retained and the "nonessential" or irrelevant degrees of freedom are "mapped out" by relaxing to their optimal values.

The proposed method is also similar to the so-called "reaction coordinate" or "constrained minimum energy path" approach, whereby a reaction path is obtained by moving along an internal coordinate and minimizing the energy with respect to all other degrees of freedom.[33] The primary difference between our method and the reaction coordinate approach is that we consider more than one mapping coordinate. It has been noted that a disadvantage of the reaction coordinate approach is that it can lead to discontinuous paths and sometimes even miss the transition state (for a review, see Ref. 33). The analysis presented in this paper shows, however, that no transition state will be missed when stiff or irrelevant degrees of freedom are mapped out. In addition, the calculation of a reaction path in the proposed method always starts from a transition state, and thus only continuous paths are obtained.

In the proposed method, the transition state is determined by the Cerjan–Miller algorithm in torsional-angle space. The reaction path is subsequently traced by following the gradient on the adiabatic surface from the transition state towards reactants and products. Due to the non-Euclidean nature of the torsional space, the gradient-following problem is formulated within the framework of Riemannian geometry. As described above, this method applies to conformational transitions in vacuum. A procedure is subsequently proposed to obtain the reaction path in solution as a "refinement" of the path determined in vacuum. To this end, molecular dynamics simulations in explicit solvent are performed with sampling orthogonal to the path in vacuum to obtain probability distributions of the orthogonal degrees of freedom. The peaks of these probability distributions then define a new path, identified as the path in solution. Finally, we propose a free energy perturbation protocol for calculating the potential of mean force along arbitrary reaction coordinates employing multidimensional internal coordinate constraints and perturbations.

II. THEORY AND COMPUTATIONAL METHODS

A. Determination of transition states on a torsional adiabatic surface

A stationary point on the full potential energy surface is a point where all first derivatives of the energy vanish. Stationary points of interest in physicochemical processes are (i) local minima, where the Hessian of the energy has all positive eigenvalues, and (ii) saddle points (or, more accurately, first-order saddle points), where the Hessian has one and only one negative eigenvalue. Local minima correspond to equilibrium points, and, as shown by Murrell and Laidler,[34] saddle points are identified with transition states (TS). The purpose of this section is to investigate the "fate" of stationary points when adiabating mapping of the full energy surface is performed. Obviously, local minima on the full surface project onto local minima on any adiabatic sur-

face, thus equilibrium points are preserved. Whether saddle points are preserved, though, is a more subtle question.

It has long been recognized that adiabatic projections (i.e., energy minimizations along a certain coordinate or coordinates) may result in discontinuous paths that miss the true transition state (see Ref. 33 and references therein). For conformational transitions, however, this is highly unlikely when the minimizations are performed with respect to bond lengths and angles. Intuitively, the true TS is missed when at that point the energy has a maximum with respect to a degree of freedom that is "mapped out." The dependence of the energy on stiff degrees of freedom does not exhibit *any* maxima, and therefore the energy can safely be minimized with respect to bond lengths and angles.

For a more detailed analysis, consider a typical empirical energy function for chain molecules (e.g., Refs. 10 and 35):

$$E(\mathbf{b},\boldsymbol{\theta},\boldsymbol{\phi}) = \sum_i K_{b_i}(b_i - b_{i0})^2 + \sum_i K_{\theta_i}(\theta_i - \theta_{i0})^2 + \sum_i K_{\phi_i}[1 + \cos(n_i\phi_i - \delta_i)] + E_N(\mathbf{b},\boldsymbol{\theta},\boldsymbol{\phi}), \tag{1}$$

where $E_N(\mathbf{b},\boldsymbol{\theta},\boldsymbol{\phi})$ is the nonbonded interaction energy,

$$E_N(\mathbf{b},\boldsymbol{\theta},\boldsymbol{\phi}) = \sum_{i,j>i} \frac{q_i q_j}{4\pi\epsilon_0 r_{ij}(\mathbf{b},\boldsymbol{\theta},\boldsymbol{\phi})} + \sum_{i,j>i}\left[\frac{A_{ij}}{r_{ij}^{12}(\mathbf{b},\boldsymbol{\theta},\boldsymbol{\phi})} - \frac{B_{ij}}{r_{ij}^{6}(\mathbf{b},\boldsymbol{\theta},\boldsymbol{\phi})}\right], \tag{2}$$

and the symbols are: $\mathbf{b} = (b_1,b_2,\ldots,b_{N-1})$: the bond lengths; $\boldsymbol{\theta} = (\theta_1,\theta_2,\ldots,\theta_{N-2})$: the bond angles; $\boldsymbol{\phi} = (\phi_1,\phi_2,\ldots,\phi_{N-3})$: the dihedral (torsional) angles; q_i,q_j: charges or partial charges; r_{ij}: interatomic distances; $K_{b_i},K_{\theta_i}K_{\phi_i}$: force constants; A_{ij},B_{ij}: parameters for the van der Waals forces; and N: the number of atoms in the molecule. Additional terms, such as improper torsions or explicit hydrogen bond terms, are commonly included but they will be omitted from the present discussion for simplicity. Improper torsion terms have a functional form similar to that for bond lengths and angles, therefore all conclusions with regard to bond lengths and angles can be extended to improper torsions as well. Hydrogen bond terms are similar in form to the van der Waals terms and can be treated in the same way. The cross terms, such as $K_{b_i\theta_i}(b_i - b_{i0})(\theta_i - \theta_{i0})$, used in some empirical energy functions only serve for fine tuning and their presence should not change the physical picture.

The nonbonded interaction energy can be expressed in terms of simple functions of the interatomic distances r_{ij}, which are completely specified for a given set of internal coordinates $(\mathbf{b},\boldsymbol{\theta},\boldsymbol{\phi})$. However, the dependence of interatomic distances on the internal coordinates is very complex, even for moderately sized molecules, and hence no further specification of the function $E_N(\mathbf{b},\boldsymbol{\theta},\boldsymbol{\theta})$ will be attempted here.

The Hessian, formed by the second derivatives of the energy with respect to the internal coordinates, can be split into blocks corresponding to bond lengths, bond angles, dihedral angles, and their mixed derivatives in the off-diagonal positions:

$$\mathbf{H} = \begin{bmatrix} \mathbf{H}_{BB} & \mathbf{H}_{B\Theta} & \mathbf{H}_{B\Phi} \\ \mathbf{H}_{\Theta B} & \mathbf{H}_{\Theta\Theta} & \mathbf{H}_{\Theta\Phi} \\ \mathbf{H}_{\Phi B} & \mathbf{H}_{\Phi\Theta} & \mathbf{H}_{\Phi\Phi} \end{bmatrix}, \tag{3}$$

where, e.g.,

$$\mathbf{H}_{BB} = \begin{bmatrix} \frac{\partial^2 E}{\partial b_1^2} & \frac{\partial^2 E}{\partial b_1 \partial b_2} & \cdots \\ \frac{\partial^2 E}{\partial b_2 \partial b_1} & \frac{\partial^2 E}{\partial b_2^2} & \cdots \\ \cdots & \cdots & \cdots \end{bmatrix}.$$

The first two terms in the right-hand side of Eq. (1) will contribute large, positive terms to the diagonal elements of $\mathbf{H}_{BB}$ and $\mathbf{H}_{\Theta\Theta}$, with an additional contribution from the nonbonded interaction energy

$$\frac{\partial^2 E}{\partial b_i^2} = 2K_{b_i} + \frac{\partial^2 E_N}{\partial b_i^2}, \tag{4a}$$

$$\frac{\partial^2 E}{\partial \theta_i^2} = 2K_{\theta_i} + \frac{\partial^2 E_N}{\partial \theta_i^2}. \tag{4b}$$

All the off-diagonal elements arise from the nonbonded interactions. If, for the moment, we neglect the contribution of the nonbonded interactions everywhere in the matrix except for $\mathbf{H}_{\Phi\Phi}$, the Hessian assumes a block-diagonal form:

$$\mathbf{H} = \begin{bmatrix} \begin{bmatrix} 2K_{b1} & & \sim 0 \\ & 2K_{b2} & \\ \sim 0 & & \cdots \end{bmatrix} & & \sim \mathbf{0} \\ & \begin{bmatrix} 2K_{\theta 1} & & \sim 0 \\ & \cdots & \\ \sim 0 & & \cdots \end{bmatrix} & \\ \sim \mathbf{0} & & [\mathbf{H}_{\Phi\Phi}] \end{bmatrix} \tag{5}$$

while $\mathbf{H}_{BB}$,$\mathbf{H}_{\Theta\Theta}$ become diagonal.

In the block diagonal form, the eigenvalues of the Hessian will simply be the eigenvalues of the component matrices, $\mathbf{H}_{BB}$, $\mathbf{H}_{\Theta\Theta}$, and $\mathbf{H}_{\Phi\Phi}$. Since $\mathbf{H}_{BB}$ and $\mathbf{H}_{\Theta\Theta}$ are diagonal, their eigenvalues will be the diagonal elements themselves, which are large and positive. Therefore, if the Hessian has one and only one negative eigenvalue, this eigenvalue must be located in $\mathbf{H}_{\Phi\Phi}$, and vice versa, if $\mathbf{H}_{\Phi\Phi}$ has one and only one negative eigenvalue, the same must be true for $\mathbf{H}$ as well.

The adiabatic mapping with respect to bond lengths and angles generates the functions $\mathbf{b}_{\text{adiab}}(\boldsymbol{\phi})$ and $\boldsymbol{\theta}_{\text{adiab}}(\boldsymbol{\phi})$ and a new surface, such that

$$E_{\text{adiab}}(\boldsymbol{\phi}) = E[\boldsymbol{\phi};\mathbf{b}_{\text{adiab}}(\boldsymbol{\phi}),\boldsymbol{\theta}_{\text{adiab}}(\boldsymbol{\phi})].$$

At any point, the curvature of the adiabatic surface will be equal to the curvature of the full surface with respect to the mapping coordinates $\boldsymbol{\phi}$, since

$$\frac{\partial E_{\text{adiab}}}{\partial \phi_i} = \frac{\partial E}{\partial \phi_i} + \sum_j \frac{\partial E}{\partial b_j}\frac{\partial b_j}{\partial \phi_i} + \sum_j \frac{\partial E}{\partial \theta_j}\frac{\partial \theta_j}{\partial \phi_i} \tag{6a}$$

and, by definition, on the adiabatic surface

$$\frac{\partial E}{\partial b_j} = \frac{\partial E}{\partial \theta_j} = 0 \quad \text{for all } j. \tag{6b}$$

(In the above equations, the derivatives of E are taken holding all other internal coordinates constant and the derivatives of E_{adiab}, b_j, and θ_j are taken holding all other torsional angles constant.) Similarly, for the second derivatives

$$\frac{\partial^2 E_{\text{adiab}}}{\partial \phi_i^2} = \frac{\partial^2 E}{\partial \phi_i^2}. \tag{6c}$$

Thus $\mathbf{H}_{\Phi\Phi} = \mathbf{H}_{\Phi\Phi,\text{adiab}}$.

The important implication of this analysis is that, if contributions of the nonbonded interactions (other than those in $\mathbf{H}_{\Phi\Phi}$) can be neglected, saddle points on the full energy surface project onto saddle points on the adiabatic surface when minimizations are performed with respect to the stiff degrees of freedom: i.e., bond lengths and angles. Conversely, saddle points on the adiabatic surface correspond to transition states on the full energy surface.

Next we address the impact of the terms in the Hessian arising from the nonbonded interactions by considering, in sequence, contributions to: (a) the diagonal elements of $\mathbf{H}_{BB}$, $\mathbf{H}_{\Theta\Theta}$; (b) the off-diagonal elements of $\mathbf{H}_{BB}$, $\mathbf{H}_{\Theta\Theta}$; and (c) the elements in $\mathbf{H}_{B\Theta}$, $\mathbf{H}_{B\Phi}$, etc.

(a) The diagonal elements of $\mathbf{H}_{BB}$ and $\mathbf{H}_{\Theta\Theta}$ are, respectively:

$$\frac{\partial^2 E}{\partial b_i^2} = 2K_{b_i} + \frac{\partial^2 E_N}{\partial b_i^2}, \tag{4a}$$

$$\frac{\partial^2 E}{\partial \theta_i^2} = 2K_{\theta_i} + \frac{\partial^2 E_N}{\partial \theta_i^2}, \tag{4b}$$

where typical values for the force constants are 300–500 Kcal/(mol Å^2) for K_{b_i} and 60–70 Kcal/(mol rad^2) for K_{θ_i}.[10] If the second derivatives of the nonbonded terms in these equations are both negative and larger than the first terms, then the diagonal elements of $\mathbf{H}_{BB}$ and $\mathbf{H}_{\Theta\Theta}$ will not necessarily be positive, which would imperil the conclusions reached in the analysis above.

It can be shown by simple geometrical arguments that

$$\left|\frac{\partial^2 E_N}{\partial b_i^2}\right| \leqslant \left|\frac{\partial^2 E_N}{\partial r^2}\right| \quad \text{and} \quad \left|\frac{\partial^2 E_N}{\partial \theta_i^2}\right| \leqslant b^2\left|\frac{\partial^2 E_N}{\partial r^2}\right|, \tag{7}$$

where b is a typical bond length. Therefore an order-of-magnitude estimate of the nonbonded contributions to the diagonal elements can be obtained by considering the second derivatives of, for example, the Lennard-Jones potential for van der Waals interactions and the Coulomb potential for electrostatic interactions. The Lennard-Jones potential is

$$U_{\text{LJ}} = \frac{A}{r^{12}} - \frac{B}{r^6},$$

where r is the interatomic distance, and typical values of A and B are 100–1000 Kcal Å^{12}/mol and 5–50 Kcal Å^6/mol, respectively.[10] The second derivative of this potential is

$$\frac{d^2 U_{\text{LJ}}}{dr^2} = 12\cdot 13\frac{A}{r^{14}} - 6\cdot 7\frac{B}{r^8},$$

and it can be seen that this derivative has large positive values at small interatomic distances and small negative values at large separations [e.g., for $A = 300$ Kcal Å^{12}/mol and $B = 10$ Kcal Å^6/mol, $(d^2U_{\text{LJ}}/dr^2) = 145$ Kcal/(mol Å^2) at $r = 1.5$ Å and -0.05 Kcal/(mol Å^2) at $r = 3$ Å]. The Coulomb potential is

$$U_{\text{el}} = \frac{q_1 q_2}{4\pi\epsilon_0 r},$$

where ϵ_0 is the permittivity of free space. If the charges are expressed in electron units, r in Å and the energy in Kcal/mol, then the second derivative is

$$\frac{d^2 U_{\text{el}}}{dr^2} = 2\cdot 331.5\frac{q_1 q_2}{r^3},$$

which is positive for like charges and negative for opposite charges. This derivative will have large absolute values at small separations [e.g., for $q_1,q_2 = +1$, $(d^2U_{\text{el}}/dr^2) = 24$ Kcal/(mol Å^2) at $r = 3$ Å and 5.3 Kcal/(mol Å^2) at $r = 5$ Å]. In most cases, q_1 and q_2 will be atomic partial charges and the numerical values of the second derivative will be smaller by 1 order of magnitude or more. Furthermore, these partial charges usually appear in groups of zero net charge, so the effects due to neighboring, opposite partial charges will tend to cancel each other, diminishing the overall contribution of the electrostatic interactions even more. Based on the analysis above, the numerical values of the second derivatives of the nonbonded interactions could never become negative *and* as large in magnitude as the force constants. Thus, the diagonal elements of $\mathbf{H}_{BB}$ and $\mathbf{H}_{\Theta\Theta}$ are always large and positive.

(b) When the off-diagonal elements in $\mathbf{H}_{BB}$ and $\mathbf{H}_{\Theta\Theta}$ are nonzero, their eigenvalues can no longer be identified with the diagonal elements of these block matrices. However, many of the off-diagonal elements will be zero since only proximal internal coordinates can give rise to nonzero off-diagonal elements. In this case, their magnitude will again be less than or equal to $(\partial^2 E_N/\partial r^2)$, which will be significantly less than the diagonal elements. Consequently, from the Gersgorin theorem in the perturbation theory of

matrices,[36] the difference between the eigenvalues and the diagonal elements is bounded by the sum of the absolute values of the off-diagonal elements of either the corresponding row or column of the matrix; i.e., if

$$\rho_j = \sum_{k \neq j} |H_{jk}| \quad \text{or} \quad \rho_j = \sum_{k \neq j} |H_{kj}|,$$

then the eigenvalues will be located within the following disks on the complex plane:

$$\{z: |z - H_{jj}| \leqslant \rho_j\} \quad j = 1,n.$$

From the analysis in part (a), all the ρ_j will be significantly smaller than the diagonal elements, and hence the eigenvalues of $\mathbf{H}_{BB}$ and $\mathbf{H}_{\Theta\Theta}$ are guaranteed to be positive.

(c) The presence of elements in $\mathbf{H}_{B\Theta}$, $\mathbf{H}_{B\Phi}$ deprives the Hessian of its block-diagonal character. However, these elements are expected to be zero or very small, and thus the Hessian will be diagonally dominant. Furthermore, the properties of matrices vary smoothly with small perturbations in their elements.[36] Therefore it is expected that the presence of these elements will not invalidate the argument made above based on the properties of block-diagonal matrices; specifically, that the eigenvalues of the Hessian will be the eigenvalues of the diagonal block matrices. It should also be noted that only the sign and not the absolute magnitude of the eigenvalues is important in the foregoing discussion.

In summary, adiabatic projections of potential energy surfaces onto the space of essential degrees of freedom retain all the information needed to identify both equilibrium and transition states for conformational transitions. The equilibrium states are determined as minima and the transition states as saddle points on this adiabatic surface.

B. Determination of the reaction path on the adiabatic surface

The definition of the IRC is the trajectory of infinitesimal velocity (or steepest descent path) from the transition state towards reactants and products.[19,20] Clearly, from this definition, a rigorous determination of the IRC should start from the transition state, from which the gradient (actually the negative of the gradient) can be followed in both directions to obtain the reaction path. This method of determining the reaction path can be adopted, even for large systems, since transition states can be readily obtained by working on adiabatic energy surfaces. For conformational transitions, the IRC determination can be simplified by an adiabatic approximation, whereby the stiff degrees of freedom are assumed to be fully relaxed at all points along the reaction path. Thus the path can be determined by following the gradient on the adiabatic surface, rather than on the full energy surface. This is the approach taken here.

One complication that frequently arises when the gradient is followed in Cartesian space is that the calculated path exhibits oscillations.[21] That is, if the path is considerably curved, any step along the gradient (the tangent to the path) will deviate from the true path, unless the step is appropriately small. As a result, the calculated path will not follow the steepest descent path, but will oscillate around it. This problem, however, is expected to be much less severe in our approach for the following reasons: First, conformational reaction paths are much less curved in internal coordinate (IC) space than in Cartesian space. For example, the reaction path for the *gauch–trans* isomerization of butane is highly curved in Cartesian space, but is almost a straight line in IC space. Second, the step along the gradient is expressed in terms of "soft" internal coordinates, so that distortion of stiff degrees of freedom, which could give rise to large gradients, does not occur. In other words, adiabatic surfaces are much "smoother" than full energy surfaces.

There has been some confusion in the literature with respect to the determination of a RP in a space other than the $3N$-dimensional Cartesian space.[37–40] If one simply follows the vector of the partial derivatives of the energy $\partial E/\partial q^i$ with respect to the coordinates used (q^i) as in Cartesian space, the path will not be the same for all coordinate sets.[37] The first instance where this problem was encountered, was in the study of triatomic collisions.[41] There, a simple coordinate transformation (the familiar "scaling and skewing" of the coordinate system) was adequate. In the general case, however, the problem of obtaining a coordinate-independent path has to be addressed within the framework of tensor calculus and Riemannian geometry.[39] A brief discussion, somewhat different from those in the literature,[20,38,39] is presented below.

In any space of generalized coordinates $\mathbf{q}$ we can define two complete sets of base vectors,[42,43] one covariant

$$\mathbf{b}_i = \sum_{k=1}^{3N} \frac{\partial x^k}{\partial q^i} \mathbf{e}_k \tag{8a}$$

and one contravariant

$$\mathbf{b}^i = \sum_{k=1}^{3N} \frac{\partial q^i}{\partial x^k} \mathbf{e}_k, \tag{8b}$$

where x^k are Cartesian coordinates and $\mathbf{e}_k$ are unit vectors along the k Cartesian axes. The gradient of the energy can be expressed in terms of either the covariant or the contravariant base vectors:

$$\text{gradient} = v^i \mathbf{b}_i = v_i \mathbf{b}^i, \tag{9}$$

where v_i and v^i are the covariant and contravariant components of the gradient, respectively, and the Einstein summation convention is used. In Cartesian space, the contravariant and covariant base vectors are identical, so no distinction between the covariant and contravariant components of the gradient can be made. Both are equal to the partial derivatives of the energy with respect to the Cartesian coordinates. However, in an arbitrary coordinate system, the partial derivatives of the energy with respect to the generalized coordinates $\mathbf{q}$ will be just the covariant components of the gradient

$$v_i = \frac{\partial E}{\partial q^i}. \tag{10}$$

In determining the reaction path in a generalized coordinate system, it is more convenient to use the covariant base vectors, since they are tangent to constant q lines, whereas the contravariant base vectors are not.[43] For example, in the case of the alanine dipeptide, where the adiabatic energy is commonly plotted as a function of the two main torsional

angles ϕ and ψ, the covariant base vectors $\mathbf{b}_\phi$ and $\mathbf{b}_\psi$ will be parallel to the ϕ and ψ axes, respectively, whereas $\mathbf{b}^\phi$ and $\mathbf{b}^\psi$ will not. However, from Eq. (9), to use the covariant base vectors, the contravariant components of the gradient are needed. These are obtained from the covariant components

$$v^i = g^{ij} v_j, \tag{11}$$

where

$$g^{ij} = \sum_{k=1}^{3N} \frac{\partial q^i}{\partial x^k} \frac{\partial q^j}{\partial x^k} \tag{12}$$

are the contravariant components of the metric tensor. This operation is in practice straightforward, since expressions for g^{ij} in terms of internal coordinates have been extensively tabulated.[53] Therefore the procedure to obtain the steepest descent path in IC space is the same as that in Cartesian space, as long as one "follows" the contravariant components of the gradient instead of the covariant components.

As discussed above, the RP is not determined in the full $(3N-6)$ dimensional IC space, but on the adiabatic energy surface in the space of "essential" torsional angles. Since movement on the adiabatic surface implies small changes in the stiff degrees of freedom, the g^{ij} should, in principle, also include contributions from these implicit changes. However, these contributions to the metric tensor will be small in magnitude and similar in all directions, so that the gradient is hardly affected. Therefore they are assumed to be negligible in the present work.

Finally, it is conceivable that the determination of the RP on the adiabatic surface instead of the full surface introduces an error, since we impose that $\partial E/\partial q^s = 0$ along the RP, where q^s is a degree of freedom that is mapped out. For stiff degrees of freedom, this will be a good approximation and the error in the steepest descent path is expected to be minimal. However, in a case where soft degrees of freedom are mapped out, the error can be significant if these degrees of freedom change substantially in the transition under study.

C. Determination of reaction paths in solution

Potential energy surfaces can be dramatically affected by the solvent, as demonstrated, for example, in studies of the alanine dipeptide in water.[44,45] Since the shape of this surface determines the reaction path, the path in solution could be dramatically different from that determined in vacuum. Present methods for calculating the RP, including the one described above, give unique, well-defined paths only for isolated molecules. When embedded in a condensed medium, however, these methods will no longer give a unique RP, but a collection of different paths, one for each local configuration of the solvent.[27]

One way to account for the effect of solvent is through some form of dielectric screening in the energy function, such as a distance-dependent dielectric constant.[27] Although this approach would hopefully bring the calculated path closer to the actual path in solution, it may not capture important solvent effects.

We propose an alternative approach whereby the path calculated in vacuum (with or without dielectric screening) is used as a zeroth-order approximation to the IRC that is subsequently refined by constrained molecular dynamics in explicit solvent. This is accomplished by constraining the molecule at different values of the RC and then sampling probability distributions in the subspace orthogonal to the path. The peaks of these probability distributions should, in principle, provide a better estimate for the path in solvent, which of course, can serve as the starting point for further refinements by the same procedure. (In principle, these refinements could be accomplished by calculating gradients of the free energy in solution. However, the uncertainties in free energy calculations do not appear to justify the computational expense of this approach.) To the extent that the simulations orthogonal to the path reproduce entropic effects, the resulting RC will essentially be a "minimum free energy" path.

In practice, sampling orthogonal to the steepest descent path is enforced by a constraint of the form[43]

$$v_i q^i = \text{constant} \quad \left(v_i = \frac{\partial E}{\partial q^i}\right), \tag{13}$$

which defines a hyperplane in IC space. A method to perform molecular dynamics simulations with single IC constraints has been proposed recently by Tobias and Brooks.[46] The method is extended here to linear combinations of ICs. Details of this algorithm are given in the Appendix. Further discussion of the orthogonal constraints is given in the next section.

D. Calculation of the free energy profile

While the energy profile for a conformational transition is simply the potential energy along the reaction path, the free energy profile (or potential of mean force) also depends on the shape of the potential energy surface in the vicinity of the reaction path. Large variations in the width of the "valley" around the reaction path will introduce significant entropic contributions to the free energy profile.

Until recently, calculations of potentials of mean force had been limited to simple reaction coordinates (e.g., Refs. 14, 17, and 47). Elber[31] has extended these calculations to general, multidimensional reaction coordinates using the free energy perturbation (FEP) method.[15,46,48] In this method, simulations are performed at successive points on the path (denoted below by 1) to sample the orthogonal degrees of freedom at each point. Perturbations to the next point on the path (denoted by 2) are then performed, and the difference in potential energy $(E_2 - E_1)$ is calculated. The free energy difference is obtained from

$$\Delta A_{1\to 2} = -kT \ln \left\langle \exp -\frac{E_2 - E_1}{kT} \right\rangle_1, \tag{14}$$

where $\langle \cdots \rangle$ denotes an ensemble average at point 1. The methodology proposed here is essentially the same; the only difference being that the constraints and perturbations are now expressed in terms of the "essential" torsional angles.

Although it is clear that sampling must be performed orthogonal to the path, the shape of the hypersurface that should be sampled is not obvious. Elber[31] chose a hyperplane in Cartesian space, and we do the same in torsional angle

space. The equation of a hyperplane orthogonal to the reaction path in torsional angle space has been given in the previous section; i.e.,

$$v_i q^i = \text{constant}.$$

A "perturbation" along the RC must move the system from points on the sampled hyperplane to points on the neighboring hyperplane corresponding to another value of the RC (see Fig. 3). Successive hyperplanes will not, in general, be parallel to each other, and hence the magnitude of the changes in torsional angles should not be equal at all points. The method adopted in this work has been to move in a direction parallel to the path, until the target hyperplane is reached. Thus perfect matching of the hyperplanes is achieved.

Since all of our work is done in torsional space, only moves of torsional angles are performed in the FEP calculation; the bond lengths and angles are kept constant during the perturbations. One might expect better sampling with this approach, since these moves involve only soft degrees of freedom, in contrast to moves in Cartesian coordinate space.

The sampling employed here is only approximately orthogonal to the path. Strictly orthogonal sampling would require bond lengths and angles to be included in the definition of the hyperplane, which is computationally much more demanding. We note, however, that such sampling has not been performed even for simple reaction coordinates. For example, in the *trans–gauche* isomerization of butane, when one constrains the torsional angle and samples all other degrees of freedom, the sampling is not strictly orthogonal, since internal coordinates are not orthogonal coordinates.[49]

III. IMPLEMENTATION

The most efficient approach to TS determination is based on the Newton–Raphson optimization scheme. This technique uses information on the second derivatives of the energy and requires diagonalization of the Hessian. It is exactly these matrix manipulations that is the bottleneck in the technique when applied to molecules with more than 20–30 atoms.[25] When Cartesian coordinates are used, the Hessian is $3N \times 3N$ dimensional, where N is the number of atoms. In contrast, the dimension of the Hessian in torsional angle space is greatly reduced, and hence these techniques become computationally more tractable.

A major shortcoming of the conventional Newton–Raphson approach is that it will converge to the closest stationary point without discriminating between saddle points and equilibrium points. Thus the method performs well when a good starting structure can be guessed (as is the case for the alanine dipeptide), but fails in more complicated situations. The algorithm proposed by Cerjan and Miller[24] and elaborated upon by Simons *et al.*[50] and by Baker[51] has been an efficient remedy to this problem. A simple form of this algorithm is implemented here: the energy is maximized along the eigenvector corresponding to the lowest eigenvalue of the Hessian and minimized along all other eigenvectors. The step along the eigenvector corresponding to the lowest eigenvalue is given by

$$h_1 = -\frac{g_1}{b_1 - \lambda_1} \qquad \lambda_1 = \frac{1}{2} b_1 + \frac{1}{2}\sqrt{b_1^2 + 4g_1^2}$$

and the step along the other eigenvectors is given by

$$h_i = -\frac{g_i}{b_i - \lambda},$$

where λ is the solution to the equation

$$\lambda = \sum_{i \neq 1} \frac{g_i^2}{\lambda - b_i},$$

b_i denotes the eigenvalues, and g_i is the projection of the gradient $[(\partial E/\partial \phi_1),(\partial E/2\phi_2),...]$ onto the eigenvector i. For comparison, the Newton–Raphson step is

$$h_i = -\frac{g_i}{b_i}.$$

The changes in the dihedral angles are then obtained as

$$\delta\phi_j = \sum_i h_i (v_i)_j,$$

where $(v_i)_j$ denotes the jth component of the eigenvector $\mathbf{v}_i$.

Two schemes were employed for the numerical evaluation of the derivatives of the adiabatic energy. In the one used initially, small displacements were performed in the mapping coordinates and the energy was minimized with respect to all other degrees of freedom. In the second, rigid-body changes in the mapping coordinates were performed and the energy was evaluated without energy minimization. By virtue of Eq. (6), the two approaches should be equivalent. Indeed, they were found to give identical results; however, for the reverse turn, the second scheme was found to be more than 20 times faster for TS determination and about 10 times faster for steepest descent path tracing. After each step in both the TS and RC determinations, the energy was minimized with respect to all other degrees of freedom, while constraining the mapping coordinates at their desired values. The adopted-basis Newton–Raphson method was used for these minimizations.[10] The diagonalization of the Hessian was performed by the Householder method.[52]

The determination of the RC is initiated by a small displacement from the transition state in either of the two directions along the eigenvector corresponding to the negative eigenvalue of the Hessian. (Rigorously, one must follow the negative eigenvalue of the matrix **HG**, where **G** is the contravariant metric tensor.[34] Since **HG** will not, in general, be symmetric, its diagonalization would be more involved.[37] In the present calculations, however, both matrices will have almost identical eigenvectors.) After that, the vector of the partial derivatives of the energy on the adiabatic surface is calculated numerically, and then multiplied by the **G** matrix for the "essential" torsional angles. The elements of the **G** matrix are calculated from the current conformation of the molecule by the expressions given by Decius.[53] A step is then taken in the direction of the resultant vector. Typical step sizes of 2.5–3 deg gave smooth paths. No stabilization procedure [e.g., see Ref. 21] was implemented. The tracing of the steepest descent path stops when the gradient vector reverses direction, signifying an equilibrium point. The values of the gradient at each point on the path are saved to be used later

as constant coefficients in the constraint equation for orthogonal sampling.

Initially, the multiple dihedral constraints were enforced during molecular dynamics simulations by a generalization of the iterative procedure of Tobias and Brooks[46] (see the Appendix). However, this procedure often failed to converge in simulations of the reverse turn, where the constraint is a combination of four dihedral angles. An alternative scheme was subsequently used, where a first estimate for the Lagrange multiplier was calculated as above, but a linear interpolation procedure was subsequently employed to obtain better estimates.

For the FEP calculations, a perturbation procedure was devised to move the system to the next hyperplane. If the moves are performed parallel to the path, then

$$\frac{\Delta\phi_1}{\Delta\phi_{10}} = \frac{\Delta\phi_2}{\Delta\phi_{20}} = \cdots = \frac{\Delta\phi_n}{\Delta\phi_{n0}},$$

where $\Delta\phi_i$ are the moves in the dihedral angles ($i = 1,...,n$) required to reach the next hyperplane, and $\Delta\phi_{i0}$ are the corresponding moves in the dihedral angles along the path (see Fig. 3). Expressing all moves in terms of $\Delta\phi_1$, we obtain

$$\Delta\phi_i = \frac{\Delta\phi_{i0}}{\Delta\phi_{10}}\Delta\phi_1. \tag{15}$$

Let v_i' be the gradient coefficients at the target hyperplane [see Eq. (13)], and ϕ_{i0}' be the values of the dihedral angles at the target point on the path. The requirement that the "perturbed" values of the dihedrals satisfy the equation of the target hyperplane leads to

$$v_1'(\phi_1 + \Delta\phi_1) + \sum_{i\neq 1} v_i'\left(\phi_i + \frac{\Delta\phi_{i0}}{\Delta\phi_{10}}\Delta\phi_1\right) = \sum_i v_i'\phi_{i0}', \tag{16}$$

where the ϕ_i are the current values of the dihedrals. Solving for $\Delta\phi_1$, we obtain

$$\Delta\phi_1 = \frac{\Sigma_i v_i'(\phi_{i0}' - \phi_i)}{v_1' + \Sigma_{i\neq 1} v_i'(\Delta\phi_{i0}/\Delta\phi_{10})}. \tag{17}$$

Equations (15) and (17) are then used to compute the required moves. "Double-wide" sampling is possible by calculating two sets of dihedral angle moves, one for the forward and one for the backward direction.

IV. APPLICATIONS

Small peptides have been useful model systems for the study of conformational properties of proteins. We have applied our method to the determination of the reaction path for the transition of the alanine dipeptide from the *c7eq* to the *c7ax* conformation, and compared the results to those previously obtained in Cartesian space.[27] The transition of a blocked alanine tripeptide from a "folded" structure mimicking reverse turns in proteins to an extended conformation was also considered. The free energy difference between the folded and unfolded conformations in water, which had been calculated previously by umbrella sampling,[54] is here obtained by FEP along the reaction path. This result reflects the intrinsically unstable nature of the reverse turn conformation, and thereby contributes to our understanding of the role of turns in the mechanism of protein folding.[54] All calculations were performed with the program CHARMM,[10] augmented with code implementing the proposed methods.

A. Alanine dipeptide

The alanine dipeptide has two primary degrees of freedom: the torsional angles ϕ and ψ around the α carbon. The other torsional angles, around the two amide bonds, always remain in their preferred, planar conformation.

Figure 1 shows the adiabatic energy surface for the alanine dipeptide with respect to ϕ and ψ. This map was obtained by minimizing the energy with respect to all other degrees of freedom at 10° intervals for ϕ and ψ. The default CHARMM energy function with a dielectric constant equal to unity was used for this calculation. The energy surface of Czerminsky and Elber,[27] which is shown in Fig. 2, was produced with a slightly different energy function. However, the portion of the map corresponding to the transition of interest, as shown in Fig. 1, is seen to be almost identical on the two surfaces.

It is apparent from Fig. 2 that all transition states determined in Cartesian space correspond to saddle points on the ϕ–ψ adiabatic surface of the alanine dipeptide, which supports the analysis in Sec. II A. Furthermore, the reaction paths on this energy surface are, for the most part, "perpendicular" to the contour lines, although deviations do exist. (The term "perpendicular" denotes "apparent" orthogonality, whereas the term "orthogonal" is used in a coordinate-independent sense.) For the path of interest here—i.e., the path connecting A and B through the transition state $T2$—these deviations become significant near the minimum energy states, A and B. Two factors can account for these deviations: the non-Cartesian nature of the ϕ–ψ space, and the fact that bond lengths and angles may not fully relax along the

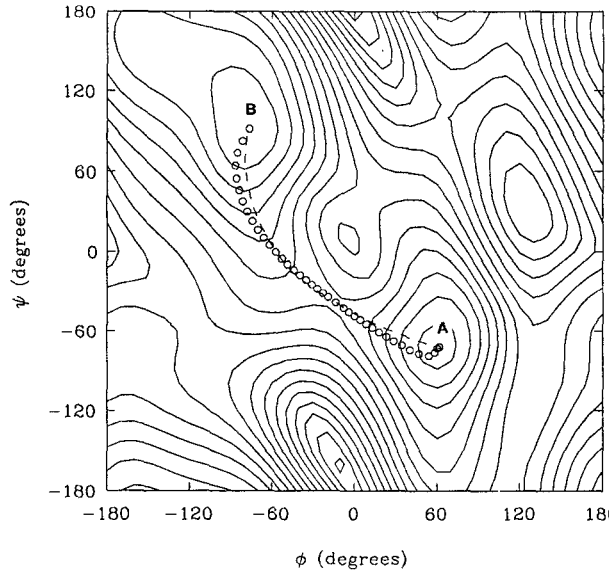

FIG. 1. Contour plot of the adiabatic energy surface with respect to the dihedral angles ϕ and ψ for the alanine dipeptide. The energy spacing between contour lines is 1.5 Kcal/mol. The circles denote the reaction path between the *c7eq* and *c7ax* conformational energy minima calculated by the present method. The dashed line is the path perpendicular to the contour lines, obtained when no use is made of the metric tensor.

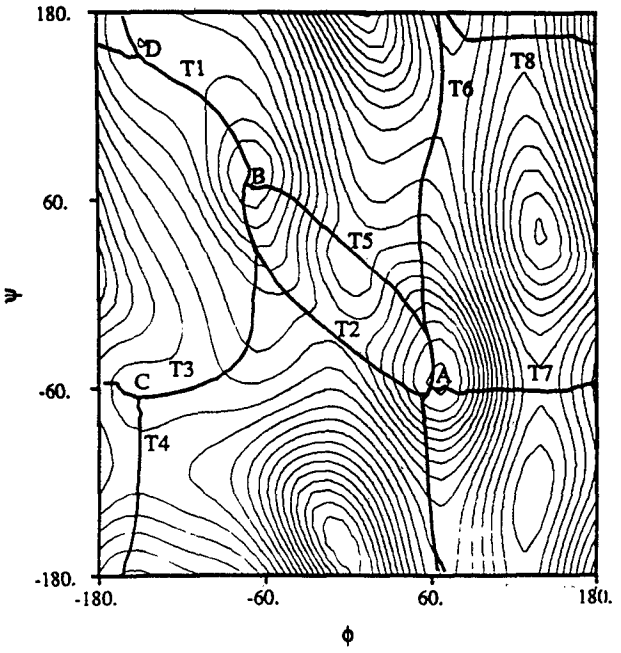

FIG. 2. Reaction paths for the alanine dipeptide calculated in Cartesian space and projected on the ϕ, ψ adiabatic energy surface. The minima are denoted by A–D and the transition states by $T1$ to $T8$ (from Ref. 27, reprinted by permission).

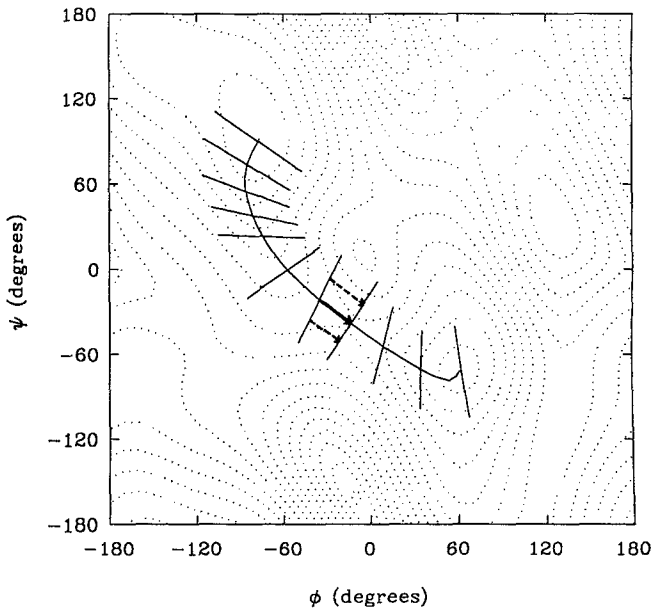

FIG. 3. Reaction path for the alanine dipeptide and the orthogonal coordinate at several points along the path. The arrows illustrate how the perturbation is performed: $\Delta\phi_0$ is denoted by the solid arrow and $\Delta\phi_i$ by the dashed arrows (see the text for details).

RC (i.e., the adiabatic approximation is not valid).

The transition state in Fig. 1 was determined on the adiabatic surface by the conventional Newton–Raphson method. The RP, determined by the method described in II B, is given by the circles in Fig. 1. Steps of 2.5 deg along the gradient were found to give a smooth path. Comparison with the path calculated in Cartesian space (Fig. 2) shows that the two results are identical. A particularly stringent comparison can be made near the equilibrium points (points A and B in Figs. 1 and 2), where the path deviates noticeably from the curve "perpendicular" to the contour lines (shown as dashed line in Fig. 1). The fact that our calculations reproduce extremely well these features of the "exact" path in Fig. 2, suggests that the deviations are due to the non-Cartesian nature of the ϕ–ψ space, and not the adiabatic approximation. Although the other paths on the alanine dipeptide map in Fig. 2 have not been determined, values of the metric tensor, calculated at selected points along these paths, have been found to account for other instances where the reaction paths are not perpendicular to the contour lines.

FEP calculations along the path in vacuum showed only a very small difference between the energy and the free energy barriers: $\Delta A = 9.12 \pm 0.5$ Kcal/mol and $\Delta E_{\text{adiab}} = 9.35$ Kcal/mol. This difference was within the estimated error of the calculation, and therefore the energy and free energy profiles are not presented here.

In order to determine the RP in water, molecular dynamics runs were performed at several points on the path in vacuum, allowing sampling of orthogonal degrees of freedom. The orthogonal coordinate at several points on the path from Fig. 1 is depicted in Fig. 3. At each point, 2000 steps of equilibration were performed, followed by 10 000 steps of production, during which the probability distribution along the orthogonal coordinate was calculated. One of these probability distributions is shown in Fig. 4, with the corresponding distribution from a run at the same point in vacuum. Although in vacuum the molecule remains close to the path, considerable deviation in the maximum and a more

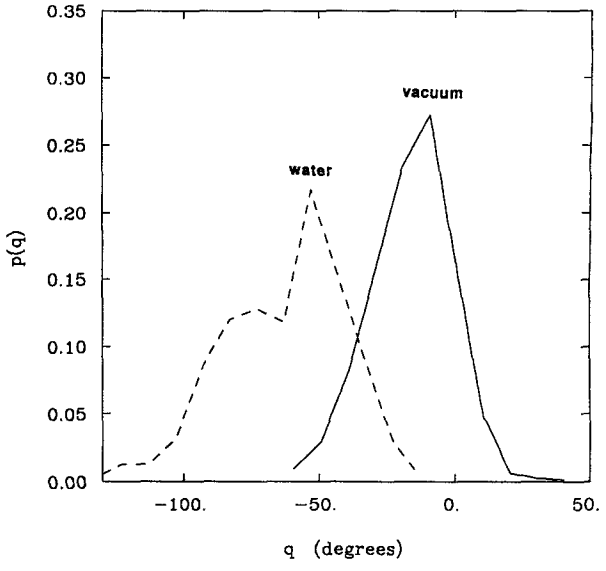

FIG. 4. Probability distribution along the orthogonal coordinate q for the alanine dipeptide in vacuum (solid line) and in explicit water (dashed line). This particular distribution was obtained at point c of Fig. 5. The value of the orthogonal coordinate is set to zero on the vacuum path.

diffuse distribution is observed in water, consistent with previous work showing that the energy surface for the alanine dipeptide in water is substantially "flatter" than in vacuum.[44] Although the characteristic shape of the probability distribution in water is also substantially different from that in vacuum, this difference may not be significant, since the simulation in water was not carried out for a sufficiently long period of time.

In principle, the peaks of the probability distributions should trace the "minimum free energy" path in water. However, the resulting path may not be very smooth since the distributions are diffuse and multiple peaks sometimes appear. Nonetheless, the peaks of the calculated distributions for the alanine dipeptide, plotted in Fig. 5, do give a clear indication of the reaction path in water. The trend is clearly towards the α-helical conformation ($\phi,\psi = -60$), which is again consistent with previous simulations, which show that the α-helical conformation is stabilized in water.[45] This trend can be attributed to the solvating function of water. For example, along line c in Fig. 5, the structure corresponding to the vacuum path exhibits a hydrogen bond between the NH and CO groups at the ends of the molecule (see Fig. 6). This bond is formed at the expense of strain in primarily the torsional angles. By examining instantaneous configurations from the constrained molecular dynamics runs in water at that point, we see that in water this intramolecular hydrogen bond is replaced by hydrogen bonds to the solvent, and thus the molecule can relax the intramolecular strain. As a result, the transition between the *c7eq* and *c7ax* conformations of the alanine dipeptide will proceed through the helical conformation. It is worth noting that this conclusion was reached here in a systematic manner, without any *ad hoc* assumptions or adjustments of the potential energy function.

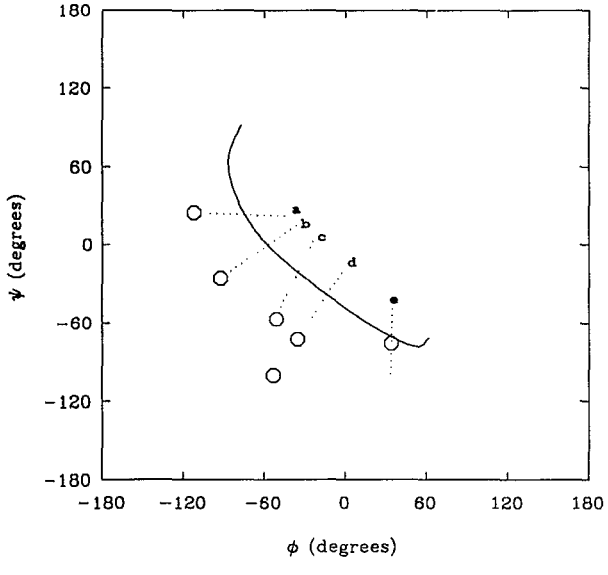

FIG. 5. Reaction path in water for the alanine dipeptide. The peaks of the probability distributions along the orthogonal coordinate are denoted by circles. The two circles in one of the orthogonal runs correspond to the two peaks of the probability distribution. For comparison, the vacuum path is shown by the solid line.

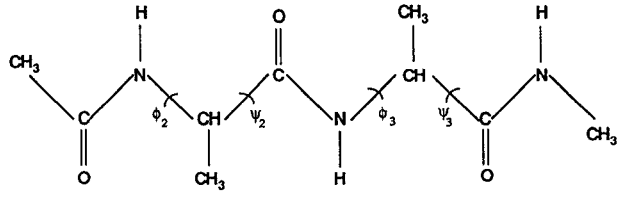

FIG. 6. The blocked alanine tripeptide used as a model for a reverse turn. The alanine dipeptide has one alanyl residue [NHCH(CH3)CO] less.

B. Reverse turn

The "alanine tripeptide" has four degrees of freedom associated with the folding process considered here: the torsional angles ϕ_2, ψ_2, ϕ_3, and ψ_3 shown in Fig. 6. Therefore the determination of the TS and the RC is performed in this four-dimensional torsional angle space. A dielectric constant of 50 was used with the expectation that the resulting path would be closer to the true path in water. This value of the dielectric constant was found to give results comparable to those of simulations with explicit water in previous (unpublished) studies on the alanine dipeptide.

The standard values of the dihedral angles for a type I reverse turn, as given by Chou and Fasman,[55] are -60, -90, -30, and 0 for ϕ_2, ψ_2, ϕ_3, and ψ_3, respectively. The corresponding values for the extended conformation are $\phi_2,\phi_3 = -120$ and ψ_2, $\psi_3 = 120$. Starting from these ideal values, a local minimum in energy was sought for each conformation. The values of the dihedral angles in the structures obtained are listed in Table I.

The Cerjan–Miller algorithm was used to search for transition states. This search was initiated from guessed structures intermediate to the two energy-minimized states, as well as from the equilibrium structures themselves. Initially a large step size was allowed (6–8 deg), which was decreased (to about 1 deg) when a region of only one negative eigenvalue was entered. The tolerance for the gradient on the adiabatic surface at the transition state was set to 0.01 Kcal/(mol rad). The increment for the numerical evaluation of the derivatives was 1 deg. After a transition state was located, the gradient was followed in both directions to give the RC and identify the equilibrium structures connected through the transition state. A total of about 3 to 5 CPU min on a Vax 3100 was required to determine a transition state starting from an arbitrary structure. The calculation of one side of a steepest descent path from a transition state to a local minimum took about 7–10 CPU min on the same machine. Thus, even though thorough code refinement and parameter optimization for the algorithm have not been attempted, the level of computational efficiency achieved is quite pleasing.

Two distinct paths resulted from the search, each proceeding through two transition states and an intermediate stable state ($M3$ and $M4$). The energy and the dihedral angles for all these equilibrium and transition states are given in Table I. The dihedral angle changes for path B in Table I are shown in Fig. 7, and the energy profile along the same path is shown in Fig. 8. All transition states were verified in the full

TABLE I. Values of the energy and the dihedral angles of the equilibrium and transition states for the unfolding of a reverse turn.

Path *A*						Path *B*					
State	Energy($\epsilon = 50$)	ϕ_2	ψ_2	ϕ_3	ψ_3	State	Energy($\epsilon = 50$)	ϕ_2	ψ_2	ϕ_3	ψ_3
*M*1	−3.15	−72.2	−37.2	−81.2	−31.3	*M*1			...		
*T*1	−1.59	−73.0	−40.4	−100.5	+56.7	*T*2	−0.98	−96.9	+44.5	−85.0	−39.1
*M*3	−2.49	−77.6	−39.3	−84.3	+130.5	*M*4	−2.22	−83.1	+131.2	−80.8	−37.9
*T*3	−0.75	−98.2	+42.8	−85.3	+129.1	*T*4	−0.81	−82.6	+130.6	−99.5	+44.2
*M*2	−2.06	−82.6	+129.2	−82.9	+129.1	*M*2			...		

Cartesian space by establishing that the Hessian (expressed in Cartesian coordinates) had one and only one negative eigenvalue.

The results in Table I and Fig. 7 show that each elementary step in the two paths involves primarily a single ψ angle. Clearly, the two paths are almost mirror images of each other. They differ only in the sequence of the changes in the ψ angles. In the first path, ψ_2 changes, followed by ψ_3. The reverse occurs in the second path. (Since only ψ_2 and ψ_3 change significantly along the paths, a reduction of the problem could be achieved by mapping out the ϕ angles as well. Trial runs showed that, indeed, the transition states could be determined equally well in the two-dimensional ψ_2, ψ_3 space.) Thus the intermediates (*M*3 and *M*4) have one ϕ, ψ pair in the α region and the other in the β region of the Ramachandran plot.[56] The transition states have one ϕ, ψ pair (the pair that is transforming) in the "bridge" region between the α and β regions, with ϕ between −95 and −100 and ψ between +45 and +55. These sequential flips were also observed by Czerminsky and Elber in their study of the helix-to-coil transition of a similar tetrapeptide[27] and by Tobias and Brooks.[57] in umbrella sampling calculations on α-helix formation.

To investigate the effect of water on this transition, we concentrate on path *B* of Table I. Molecular dynamics simulations in explicit water were performed at 14 points along the path and probability distributions for the four angles were calculated. [Strictly speaking, a three-dimensional probability distribution $p(q_1,q_2,q_3)$ should be calculated, where q_i are properly defined normal coordinates. However, due to practical difficulties in determining normal coordinates and calculating a multivariate distribution, we simply resorted here to calculating the distributions of the four angles $p(\phi_2)$,$p(\psi_2)$,$p(\phi_3)$, and $p(\psi_3)$. This approximation may, in principle, contribute somewhat to the scatter of the peaks of the distributions plotted in Fig. 8.] The peptide was placed in a 15×31 Å rectangular box of 250 equilibrated TIP3P waters and all water molecules overlapping with peptide atoms were deleted. Periodic boundary conditions were employed. The system was equilibrated for 2000 steps and 10 000 additional steps were used to calculate the probability distributions (time step = 1.5 fs and SHAKE for all bonds with hydrogens). These simulations were performed on the Cray-YMP at the Pittsburgh Supercomputer Center. The peaks of the calculated distributions are plotted in Fig. 7. No systematic deviation from the original profile in high-dielectric vacuum is observed, except perhaps for the ϕ_3 angle near TS4. This deviation is probably due to a hydrogen bond be-

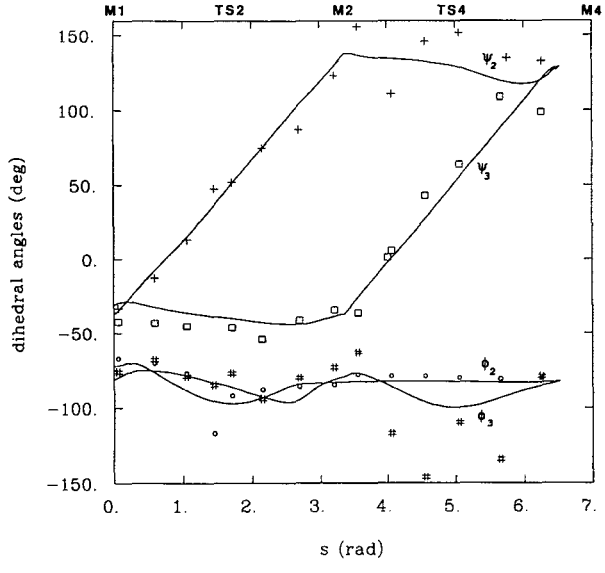

FIG. 7. Dihedral angle profile along path *B* for the reverse turn (solid lines) and the peaks of the probability distributions for the same angles from the orthogonal runs in water ϕ_2 (O), ψ_2 (+), ϕ_3 (#), ψ_3 (□). The top scale indicates the stationary states along the path. The arc length in radians along the path is denoted by *s*.

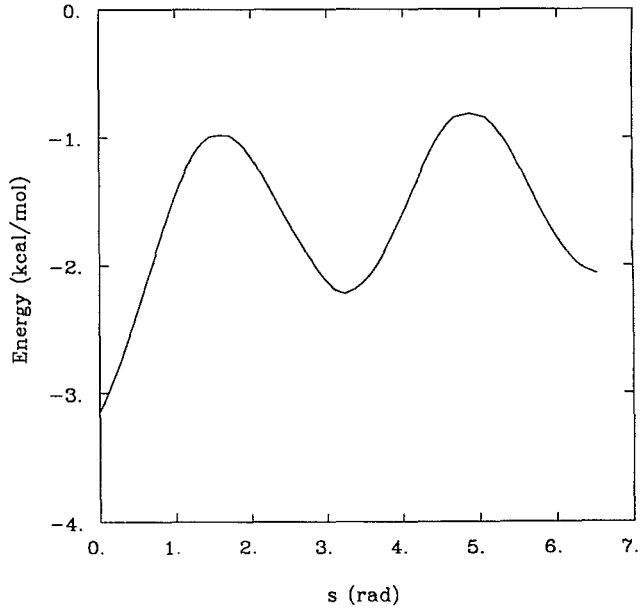

FIG. 8. The potential energy profile along path *B* for the reverse turn.

tween the NH–methyl blocking group and the central carbonyl group, which is present in the initial path but can be replaced by hydrogen bonds to water in the simulations. Apparently, the sequential mechanism of the transition is not affected by water. Overall, the high-dielectric vacuum path seems to be a good approximation for the actual path in water and therefore was used as the basis for the FEP study.

A total of 132 points were selected along the path for the FEP calculations in water. Simulations were performed at every other point with double-wide perturbations to both neighboring hyperplanes, so that the entire path was covered. The advantage of an equal number of "forward" and "backward" perturbations in the construction of the free energy profile is that systematic errors due to, for example, the magnitude of the perturbation tend to cancel each other. The changes in the dihedral angles required to move parallel to the path from one hyperplane to another were calculated as described in Sec. III. Typical values for these changes near the path are 2–3 deg for the primary angle (ψ_2 or ψ_3) and 0.5 to 1 deg for the other angles. Far from the path, though, the changes may become larger, as the orthogonal hyperplanes are not parallel to each other.

The simulations were initiated with the peptide structure on the path and solvated in a box of equilibrated water molecules, as above. The equilibration consisted of 2000 steps (3 ps), followed by 15 000 steps (22.5 ps) of sampling. The velocities were rescaled every 200 steps to maintain a temperature of 300 K. "Perturbations" were performed at every other step. The 66 simulations required about 60 single-processor CPU h on the CRAY-YMP.

Standard deviations of the mean for individual FEP runs, calculated by splitting the sample into bins of 100 data points each, were quite large (about 30% on average). However, this should be expected, since the peptide samples a wide range of configurations during a simulation, and each is likely to exhibit slightly different solvation properties. The excursions of the molecule away from the path were quite large (certain dihedral angles varied by *more than 180 deg in some runs*). This demonstrates the great flexibility of these peptides and suggests that a diffusive description of their conformational transitions might be more appropriate.

By splicing together the calculated free energy differences, the free energy profile in Fig. 9 is obtained. The two barriers are slightly shifted to lower values of the reaction coordinate *s*, compared to the energy profile in Fig. 8. The magnitude of the first barrier is 2.77 and that of the second 2.34 Kcal/mol. The major difference between Figs. 8 and 9 is in the relative stability of the equilibrium states. The unfolded state in water is found to be more stable than the folded state by about 3.1 Kcal/mol., which is in qualitative agreement with the value of 5 Kcal/mol estimated by umbrella sampling.[54] The discrepancy between the two methods is understandable, given the large uncertainties inherent in free energy calculations.

Unfortunately, the result obtained on the relative stability of the folded and unfolded states cannot be regarded as highly reliable, since a large number of intermediate calculations were needed to obtain this result. Errors in the intermediate calculations may easily accumulate and shift considerably the free energy difference. More and longer simulations are required to diminish the uncertainty of the results. Another factor that needs to be included for improved accuracy is a "momentum correction," that arises because the momentum conjugate to the reaction coordinate is forced to be zero during the simulation.[58] However, this correction should be rather small compared to the other uncertainties in the calculation. Further analysis of the contributions to the free energy barrier and free energy differences of intramolecular and intermolecular (solvation) interactions, electrostatic interactions, peptide vibrational entropy, etc., as well as the effect of different side chains, would be essential in understanding the source of the instability of the folded conformation. This analysis will be pursued in future work.

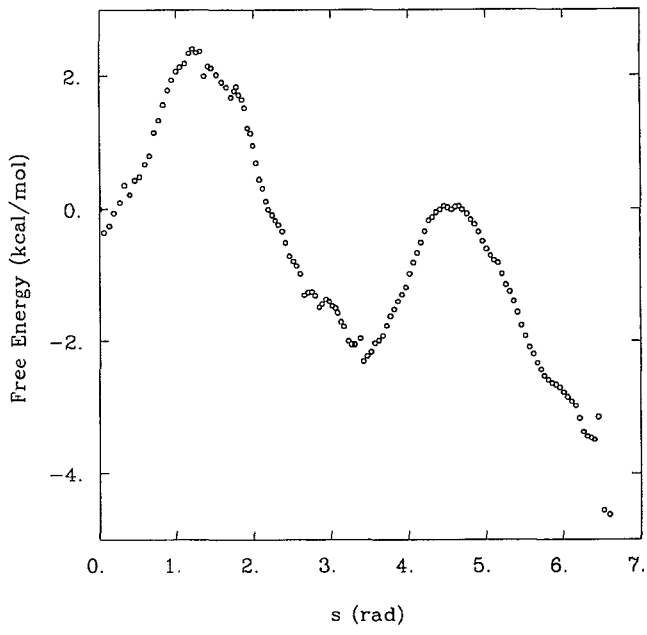

FIG. 9. The free energy profile along path *B* for the reverse turn in water.

V. CONCLUSIONS

The proposed method has been shown to be an efficient route to the determination of transition states for conformational transitions. The reaction paths obtained here appear to be as accurate as those calculated by conventional methods in Cartesian space. For small molecules, such as the alanine dipeptide, conventional methods are quite satisfactory and the advantages offered by the present method will be marginal. However, its necessity for larger systems can be clearly recognized. Although the energy minimizations required in our approach represent an additional computational expense, they do not scale as dramatically with system size as do matrix manipulations. Application of the method to the dynamics of an inhibitor bound to the active site of chymotrypsin is currently underway.[59]

Although the proposed method is most useful in studies of conformational transitions, specifically those involving torsional angles, it is not restricted to these problems or to empirical energy surfaces. The basic ideas are valid in any reaction where certain degrees of freedom are not directly

involved and adjust only slightly within a narrow potential energy well. In cases where covalent bonds or angles are severely distorted, the algorithm would have to be extended in order to allow for such degrees of freedom to be treated explicitly as essential degrees of freedom. Another useful extension would be the incorporation of intermolecular interactions, i.e., the ability to study physical interactions between two or more molecules. In that case, the set of essential internal degrees of freedom would need to be complemented by the intermolecular distances and relative orientations of the molecules.

Although costly, constrained simulations in explicit solvent seem to provide the most rigorous, systematic way to obtain reaction paths in solution. Good first estimates, however, may be obtained by the use of higher dielectric constants (or distance-dependent dielectric constants[27]). Application to the reverse turn model showed that the sequential mechanism of conformational transitions in peptides is not affected by water. However, water was found to strongly affect the relative stability of the folded and unfolded conformations of the peptide.

The determination of conformational free energy profiles and relative stabilities by FEP is feasible, although large amounts of computer time are required to obtain reliable thermodynamic quantities. The FEP method can be easily applied to larger molecules, as long as the "moved" group is small, such as an aromatic ring.[59] Its applicability, however, is questionable when large parts of the molecule, such as a whole α-helix, must be moved. The development of reliable, alternative techniques for the calculation of free energy differences between different conformational states, ideally without the need of intermediate simulations, would obviously be of great utility.

ACKNOWLEDGMENTS

This work was supported by the National Science Foundation (Grant No. CPE 8351228). Computational support has been provided by CRAY Research, Inc. (Grant No. CBT900011P) at the Pittsburgh Supercomputer Center. We are grateful to Professor R. Elber for sharing with us his computer codes and preprints of his work. T. L. would like to thank Eric Boczko for his hospitality during the former's stay in Pittsburgh. C. L. B. III acknowledges the National Institute of Health (Grant No. GM37554) and the National Science Foundation (Grant No. ASC8916093) for partial support of this work. C. L. B. III is an Alfred P. Sloan Fellow, 1990–1992.

APPENDIX

In this Appendix we formulate the problem of performing molecular dynamics simulations subject to a constraint of a linear combination of internal coordinates. This is an extension of the approach of Tobias and Brooks[46] for single internal coordinate constraints, which, in turn, was based on the SHAKE algorithm.[60] For more details the reader is referred to Ref. 46.

Consider the holonomic constraint

$$\sigma = \sum_{k=1}^{l} v_k S_k - \sum_{k=1}^{l} v_k S_k^0 = \sum_{k=1}^{l} v_k \delta S_k = 0, \tag{A1}$$

where S_k are internal coordinates and v_k are constant coefficients. The Lagrange equations of the first kind are

$$m_i \mathbf{a}_i = -\nabla_i U - \lambda \nabla_i \sigma \quad i = 1, \cdots N, \tag{A2}$$

where m_i and $\mathbf{a}_i$ are the mass and the acceleration, respectively, of particle i and λ is an unknown Lagrange multiplier. The solution of the above equation at time step h is

$$\mathbf{r}_i(h) = \mathbf{r}_i'(h) + \delta \mathbf{r}_i(h), \tag{A3}$$

where $\mathbf{r}_i'$ is the solution to the unconstrained problem, and the $\delta \mathbf{r}_i$ are the Cartesian displacements that need to be added to satisfy the constraint

$$\delta \mathbf{r}_i(h) = \frac{h^2}{m_i} \lambda \nabla_i \sigma. \tag{A4}$$

For small displacements, as those occurring over one molecular dynamics step, the internal coordinates can be approximated as linear functions of the Cartesian coordinates of the atoms defining them:

$$\delta S_k = \sum_{j=1}^{n_k} \mathbf{s}_{kj} \cdot [\mathbf{r}_j(h) - \mathbf{r}_j(0)], \tag{A5}$$

where n_k is the number of atoms defining the IC and $\mathbf{s}_{ki}$ is the Wilson vector[49] for the ith atom in the k th IC. The gradient of the constraint is

$$\nabla_i \sigma = \sum_{k=1}^{l} v_k \mathbf{s}_{ki}. \tag{A6}$$

Using Eq. (A3), Eq. (A1) becomes

$$\sigma = \sum_{k=1}^{1} v_k \sum_{j=1}^{n_k} \mathbf{s}_{kj} \cdot [\mathbf{r}_j'(h) + \delta \mathbf{r}_j(h) - \mathbf{r}_j(0)] = 0. \tag{A7}$$

The last equation can be written

$$\sum_{k=1}^{l} v_k \sum_{j=1}^{n_k} \mathbf{s}_{kj} \cdot \delta \mathbf{r}_j(h) = -\sum_{k=1}^{l} v_k \delta S_k', \tag{A8}$$

where

$$\delta S_k' = \sum_{j=1}^{n_k} \mathbf{s}_{kj} \cdot [\mathbf{r}_j'(h) - \mathbf{r}_j(0)]. \tag{A9}$$

Substituting Eq. (A4) into Eq. (A8) we obtain

$$\sum_{k=1}^{l} v_k \sum_{j=1}^{n_k} \mathbf{s}_{kj} \cdot \left(\frac{h^2}{m_j} \lambda \nabla_j \sigma\right) = -\sum_{k=1}^{l} v_k \delta S_k', \tag{A10}$$

which can be solved for λ, using also Eq. (A6):

$$\lambda h^2 = \frac{-\Sigma_{k=1}^{l} v_k \delta S_k'}{\Sigma_{k=1}^{l} v_k \Sigma_{j=1}^{n_k} (1/m_j) \mathbf{s}_{kj} \cdot (\Sigma_{k'=1}^{l} v_{k'} \mathbf{s}_{k'j})}. \tag{A11}$$

The desired displacements are then obtained from Eq. (A4).

The numerator of Eq. (A11) can be easily calculated from Eq. (A9). The denominator can be decomposed into $k = k'$ and $k \neq k'$ contributions, for more convenient implementation:

$$\sum_{k=1}^{l} v_k \sum_{j=1}^{n_k} \frac{1}{m_j} \mathbf{s}_{kj} \cdot \left(\sum_{k'=1}^{l} v_{k'} \cdot \mathbf{s}_{k'j} \right)$$
$$= \sum_{k=1}^{l} v_k^2 \sum_{j=1}^{n_k} \frac{1}{m_j} \mathbf{s}_{kj}^2$$
$$+ 2 \sum_{k=1}^{l} \sum_{k'>k}^{1} v_k v_{k'} \sum_{j=1}^{n_{com}} \frac{1}{m_j} \mathbf{s}_{kj} \cdot \mathbf{s}_{k'j}, \quad \text{(A12)}$$

where n_{com} is the number of common atoms in internal coordinates k and k' (the summation is performed only over common atoms because either $\mathbf{s}_{kj}$ or $\mathbf{s}_{k'j}$ will be zero for all others). The factor of 2 in the last term of Eq. (A12) compensates for summing over $k' > k$ instead of $k' \neq k$ in the same term.

[1] A. J. Hopfinger, *Conformational Properties of Macromolecules* (Academic, New York, 1973).
[2] P. J. Flory, *Statistical Mechanics of Chain Molecules* (Interscience, New York, 1969).
[3] T. E. Creighton, *Proteins, Structure and Molecular Properties* (Freeman, New York, 1984).
[4] W. P. Jencks, *Catalysis in Chemistry and Enzymology* (Dover, New York, 1969).
[5] P. G. Debrunner and H. Frauenfelder, Ann. Rev. Phys. Chem. **33**, 283 (1982); M. Karplus and J. A. McCammon, Ann. Rev. Biochem. **53**, 263 (1983).
[6] R. Cook, J. Polym. Sci., Polym. Phys. Ed. **26**, 1337 (1988); T. Bleha, J. Gajdos, and F. E. Karasz, Macromolecules **23**, 4076 (1990).
[7] E. Helfand, Science **226**, 647 (1984).
[8] J. Schaefer, E. O. Stejaskal, and R. Buchdahl, Macromolecules **10**, 384 (1977); M. D. Sefcik, J. Schaefer, F. L. May, D. Raucher, and S. M. Dub, J. Polym. Sci. **21**, 1041 (1983).
[9] M. W. Hellums, W. J. Koros, and D. R. Paul, AICHE Symp. Ser. **85**, 6 (1989).
[10] B. R. Brooks, R. E. Bruccoleri, B. D. Olafson, D. J. States, S. Swaminathan, and M. Karplus, J. Comput. Chem. **4**, 187 (1983).
[11] C. H. Bennett, in *Algorithms for Chemical Computations*, edited by R. E. Christofferson (American Chemical Society, Washington, D.C., 1977), pp. 63–97.
[12] D. Chandler, J. Chem. Phys. **68**, 2959 (1978).
[13] *Computer Simulations of Biomolecular Systems*, edited by W. F. van Gunsteren and P. K. Weiner (ESCOM, Leiden, 1989).
[14] S. H. Northrup, M. R. Pear, C. -Y. Lee, J. A. McCammon, and M. Karplus, Proc. Natl. Acad. Sci. U.S.A. **79**, 4035 (1982).
[15] W. L. Jorgensen and J. K. Buckner, J. Phys. Chem. **91**, 6083 (1987).
[16] R. O. Rosenberg, R. Mikkilineni, and B. J. Berne, J. Am. Chem. Soc. **104**, 7647 (1982).
[17] W. L. Jorgensen, J. Chem. Phys. **77**, 5757 (1982).
[18] J. Kottalam and D. A. Case, J. Am. Chem. Soc. **110**, 7690 (1988).
[19] K. Fukui, J. Phys. Chem. **74**, 4161 (1970).
[20] K. Fukui, Acc. Chem. Res. **14**, 363 (1981).
[21] K. Ishida, K. Morokuma, and A. Komornicki, J. Chem. Phys. **66**, 2153 (1977).
[22] M. W. Schmidt, M. S. Gordon, and M. Dupuis, J. Am. Chem. Soc. **107**, 2585 (1985).
[23] S. Bell and J. S. Crighton, J. Chem. Phys. **80**, 2464 (1984).
[24] C. J. Cerjan and W. H. Miller, J. Chem. Phys. **75**, 2800 (1981).
[25] D. T. Nguyen and D. A. Case, J. Phys. Chem. **89**, 4020 (1985).
[26] R. Czerminski and R. Elber, Proc. Natl. Acad. Sci. U.S.A. **86**, 6963 (1989).
[27] R. Czerminski and R. Elber, J. Chem. Phys. **92**, 5580 (1990).
[28] C. Choi and R. Elber, J. Chem. Phys. **94**, 751 (1991).
[29] W. Nowak, R. Czerminski, and R. Elber, J. Am. Chem. Soc. **113**, 5627 (1991).
[30] R. Elber and M. Karplus, Chem. Phys. Lett. **139**, 375 (1987).
[31] R. Elber, J. Chem. Phys. **93**, 4312 (1990).
[32] B. R. Gelin, and M. Karplus, Proc. Natl. Acad. Sci. U.S.A. **72**, 2002 (1975).
[33] K. Muller, Angew. Chem. Int. Ed. Engl. **19**, 1 (1980).
[34] J. N. Murrel and K. J. Laidler, Trans. Faraday Soc. **64**, 371 (1968).
[35] S. J. Weiner, P. A. Kollman, D. A. Case, U. C. Singh, C. Chio, G. Alagona, S. Profeta, Jr., and P. Weiner, J. Am. Chem. Soc. **106**, 765 (1984).
[36] J. H. Wilkinson, *The Algebraic Eigenvalue Problem* (Clarendon, Oxford, 1965), p. 71.
[37] M. Sana, G. Reckinger, and G. Leroy, Theor. Chim. Acta **58**, 145 (1981).
[38] A. Nauts and X. Chapuisat, Chem. Phys. Lett. **85**, 212 (1982).
[39] W. Quapp and D. Heidrich, Theor. Chim. Acta **66**, 245 (1984).
[40] G. A. Natanson, Mol. Phys. **46**, 481 (1982).
[41] S. Goldstein, K. J. Laidler, and H. Eyring, *The Theory of Rate Processes* (McGraw Hill, New York, 1941).
[42] T. C. Bradbury, *Theoretical Mechanics* (Wiley, New York, 1968), pp. 65–76.
[43] L. P. Eisenhart, *Riemannian Geometry* (Princeton University, Princeton, 1963).
[44] B. M. Pettitt and M. Karplus, Chem. Phys. Lett. **21**, 194 (1985).
[45] M. Mezei, P. K. Mehrotra, and D. L. Beveridge, J. Am. Chem. Soc. **107**, 2239 (1985).
[46] D. J. Tobias and C. L. Brooks III, J. Chem. Phys. **89**, 5115 (1988).
[47] G. Ravishanker, M. Mezei, and D. L. Beveridge, Faraday Symp. Chem. Soc. **17**, 79 (1982).
[48] W. L. Jorgensen, J. K. Buckner, S. Boudon, and J. Tirado-Rives, J. Chem. Phys. **89**, 3742 (1988).
[49] E. B. Wilson, J. C. Decius, and P. C. Cross, *Molecular Vibrations* (Dover, New York, 1955).
[50] J. Simons, P. Jorgensen, H. Taylor, and J. Ozment, J. Phys. Chem. **87**, 2745 (1983); A. Banerjee, N. Adams, J. Simons, and R. Shepard, J. Phys. Chem. **89**, 52 (1985).
[51] J. Baker, J. Comput. Chem. **7**, 385 (1986).
[52] W. H. Press, B. P. Flannery, S. A. Teukolsky, and W. T. Vetterling, *Numerical Recipes* (Cambridge University, Cambridge, 1986), p. 350.
[53] J. C. Decius, J. Chem. Phys. **16**, 1025 (1948).
[54] D. J. Tobias, S. F. Sneddon, and C. L. Brooks III, J. Mol. Biol. **216**, 783 (1990).
[55] P. Y. Chou and G. D. Fasman, J. Mol. Biol. **115**, 135 (1977).
[56] J. S. Richardson, Adv. Protein Chem. **34**, 168 (1981).
[57] D. J. Tobias and C. L. Brooks III, Biochemistry **30**, 6059 (1991).
[58] H. J. C Berendsen and W. F. van Gunsteren, in *The Physics of Superionic Conductors and Electrode Materials*, edited by J. W. Perram, NATO ASI B92 (Plenum, New York, 1983), p. 221; E. A. Carter, G. Ciccotti, J. T. Hynes, and R. Kapral, Chem. Phys. Lett. **156**, 472 (1989).
[59] T. Lazaridis and M. E. Paulaitis (work in progress).
[60] J. -P. Ryckaert, G. Ciccotti, and H. J. C. Berendsen, J. Comput. Phys. **23**, 327 (1977).